photonics

MDPI

Article

Flexible Construction of a Partially Coherent Optical Array

Kaiqi Zhu [1,2], Yilin Wu [1,2], Mengdi Li [1,2], Xiaofei Li [3], Yaru Gao [1,2] and Xianlong Liu [1,2,*]

[1] Shandong Provincial Engineering and Technical Center of Light Manipulation & Shandong Provincial Key Laboratory of Optics and Photonic Devices, School of Physics and Electronics, Shandong Normal University, Jinan 250358, China; gaoyaru@sdnu.edu.cn (Y.G.)
[2] Collaborative Innovation Center of Light Manipulations and Applications, Shandong Normal University, Jinan 250358, China
[3] Department of Electrical and Computer Engineering, Dalhousie University, Halifax, NS B3J 2X4, Canada
* Correspondence: xianlongliu@sdnu.edu.cn

Abstract: In this article, we introduce a flexible and programmable method to construct a multi-parameter optical array to meet urgent and personalized needs, such as multi-particle capture and manipulation and material processing, and enrich the degree of freedom when constructing an optical array. As an example, uniform and nonuniform spiral coherent lattices (SCLs) and their propagation properties are investigated both theoretically and experimentally. Various intensity distributions, e.g., a uniform and nonuniform spiral light field, can be achieved by manipulating the diverse parameters. Additionally, the complex degree of coherence exhibits phase singularities in the source plane, which can be used for constructing optical vortex beams.

Keywords: coherence; optical coherence lattices; propagation

Citation: Zhu, K.; Wu, Y.; Li, M.; Li, X.; Gao, Y.; Liu, X. Flexible Construction of a Partially Coherent Optical Array. *Photonics* **2024**, *11*, 133. https://doi.org/10.3390/photonics11020133

Received: 5 January 2024
Revised: 26 January 2024
Accepted: 29 January 2024
Published: 31 January 2024

1. Introduction

Since Gori et al. proposed sufficient conditions for constructing partially coherent beams [1,2], various partially coherent beams have been proposed, with different amplitude distributions [3,4] and spatial coherent structures [5,6] and carrying different phases [7,8]. The partially coherent beams can be classified through response functions; when the response functions of these two systems are different, they can be divided into uniformly correlated partially coherent beams and non-uniformly correlated partially coherent beams [9,10]. In addition, there is a special type of partially coherent beam that carries a twist phase which can be observed through the reasonable adjustment of the system response function [11]. Among them, the complex degree of coherence of uniformly correlated partially coherent beams depends on the absolute position of two points in space, which can also be referred to as partially coherent Schell model beams. After determining the system response function, multiple special correlated partially coherent beams can be generated by designing weight functions. The Gaussian Schell model beam constructed by Collett and Wolf in 1978, as a classical correlated partially coherent beam, has been extensively studied for its generation, transmission, and application [12,13]. As research progresses, various partially coherent beams, including scalar and vector partially coherent beams, have been discovered and widely applied. These beams exhibit unique properties during propagation, including self-healing [14], self-focusing [15], self-splitting [16], and self-shifting [17] properties, and they show extraordinary advantages in overcoming random perturbation when propagating through random media, such as turbulent atmosphere [18], turbulent ocean [19], and weak scattering [20]. Partially coherent beams can be used to improve image quality in classical or correlation images [21] or to reduce bit error rates [22] and have found potential use in laser processes [23], robust imaging through random media [24], and free-space optical communication [25–27].

Recently, research on optical arrays has received increasing attention; various optical arrays have been proposed to cater to practical applications, and currently there are many

methods for generating optical array. Usually, a spatial light modulator is used to modulate the beam to construct various optical arrays, as this method is not only simple but also efficient [28,29]. Optical arrays have demonstrated their usefulness in many aspects, such as beam shaping [30], lattice light microscopy [31], and as a universal tool for performing quantum simulations [32]. However, all these discussions are based on completely coherent beam modulation. As typical partially coherent sources, optical coherent lattices have attracted great attention in recent years. Since Sergey et al. introduced the optical coherent lattices mode [33], vector optical coherent lattices [34] and the carrying vortex phase [35], as well as experimental generation [36] and paraxial propagation [37] through random media [19,38], have been studied extensively. The periodicity reciprocity arises between the source coherence and far-zone intensity of optical coherence lattices during propagation. The periodicity reciprocity of optical coherent lattices mean a Gaussian intensity profile of an optical coherence lattices evolves into a lattice-like far-field profile, while the periodic spectral degree of coherence at the source loses its periodicity during propagation [37]. The periodic reciprocity of optical coherent lattices has shown great potential use for the aspects of orientation-selective sub-Rayleigh imaging [39], free space optical communication [37], and optical encryption [36]. Recent research has shown that one can generate perfect optical coherent lattices [40] and tunable polarization optical arrays [41], which indicates that flexible and programmable optical coherent arrays extend the scope of application and are now becoming a future trend.

A typical feature of a vortex beam is the circular symmetry distribution of intensity distribution in the dark, with a continuous spiral phase distribution and an uncertain phase at the center point, which is called phase singularity [42]. The expression for vortex phase is $\exp(il\varphi)$; l represents the direction of phase distortion, with a positive sign corresponding to counterclockwise distortion and a negative sign corresponding to clockwise distortion. Since its discovery, vortex beams have been extensively studied due to their wide range of applications. Recent studies have shown that vortex beams can be applied in free space optical communication [43], particle capture [44], microscopy imaging [45], astrometry [46], and other fields. To cope with application environments in different fields, high-quality vortex beam generation important. There are currently many methods for generating vortex beams, and the most commonly used methods are those using spiral phase plates (SPPs) [47,48] and spatial light modulators (SLMs) [28]. Given some new applications of vortex beams, such as polarization detection [49] and edge enhancement images [50], the generation of vortex beams has become increasingly important. However, is it possible to construct a vortex beam without utilizing the vortex phase? Recently, research has shown that high-quality vortex beams can be generated by using a gradual-width Fermat spiral slit mask [51]. In this article, we were surprised to discover phase singularities in the CDOC phase distribution of the source plane of SCLs, which may be useful for constructing vortex beams in the future without utilizing the vortex phase.

In this article, we propose a flexible and programmable method for constructing optical coherent lattices by manipulating the initial coherence structure. This method can modify the generated optical array from aspects of the spatial structure, such as the amplitude or the size of individual light spots, and the number and individual position of the light spots. A spiral structure array and its propagation properties are studied in detail as examples, by manipulating the initial beam parameters, e.g., the coherent length, and a spiral-like beam field can be achieved in the far field. We also discovered phase singularities in the phase distribution of CDOC in the source plane. Our discovery is useful for constructing vortex beams without the vortex phase. Therefore, through our proposed method, optical array can be flexibly modified to meet the requirements of diverse usage scenarios.

2. Methods

We began with the construction of the partially coherent beam sources. In the space-frequency domain, partially coherent beams can be characterized by the cross-spectral density (CSD) function of the electric field, which is defined as [1]:

$$W_o(\mathbf{r}_1, \mathbf{r}_2) = \int \mathrm{I}(\mathbf{v}) H^*(\mathbf{r}_1, \mathbf{v}) H(\mathbf{r}_2, \mathbf{v}) d^2\mathbf{v} \tag{1}$$

where $\mathbf{r}_1$ and $\mathbf{r}_2$ are two arbitrary spatial points at the source plane, with '*' denoting the complex conjugate. $\mathrm{I}(\mathbf{v})$ is a non-negative function. $H(\mathbf{r}, \mathbf{v})$ is an arbitrary kernel. Equation (1) can be rewritten as an alternative form to facilitate experimental generation [35]:

$$W_o(\mathbf{r}_1, \mathbf{r}_2) = \int\int W_i(\mathbf{v}_1, \mathbf{v}_2) H^*(\mathbf{r}_1, \mathbf{v}_1) H(\mathbf{r}_2, \mathbf{v}_2) d^2\mathbf{v}_1 d^2\mathbf{v}_2, \tag{2}$$

with

$$W_i(\mathbf{v}_1, \mathbf{v}_2) = \sqrt{\mathrm{I}(\mathbf{v}_1)\mathrm{I}(\mathbf{v}_2)}\,\delta(\mathbf{v}_1 - \mathbf{v}_2), \tag{3}$$

where $W_i(\mathbf{v}_1, \mathbf{v}_2)$ and $W_o(\mathbf{r}_1, \mathbf{r}_2)$ denote the CSD functions in the input and output planes, respectively. The terms $\mathrm{I}(\mathbf{v})$, $\delta(\mathbf{v}_1 - \mathbf{v}_2)$, and $H(\mathbf{r}, \mathbf{v})$ correspond to the intensity, the delta function, and the response function of the optical system, respectively. Based on Equation (2), one can achieve any partially coherent beams desired by flexibly editing the $\mathrm{I}(\mathbf{v})$ or $H(\mathbf{r}, \mathbf{v})$ functions. A coherent lattice with its incoherent intensity distribution is expressed as [35]:

$$\mathrm{I}(\mathbf{v}) = C_0 \sum_{m=1}^{M} c_m \exp\left[-\frac{(\mathbf{v} - \mathbf{v}_{0m})^2}{\omega_m^2/2}\right], \tag{4}$$

where C_0 is a constant factor, M is a non-negative integer denoting the number of Gaussian beam spots, c_m is the weight coefficient, which is used to adjust amplitude distribution, ω_m is the beam waist size of the Gaussian beam spot, and $\mathbf{v}_{0m} = (v_{0mx}, v_{0my})$ is the off-axis displacement of the mth spot. Additionally, by manipulating the weight coefficient c_m, the beam waist size ω_m, and the off-axis displacement $\mathbf{v}_{0m}$, arrays can be flexibly implemented through programming.

Spiral coherent lattices (SCLs) can be obtained from the incoherent intensity distribution, which is shaped as an Archimedes spiral distribution, with its off-axis displacement $\mathbf{v}_{0m}$ expressed as:

$$\mathrm{v}_{0mx} = a_m \cos(t_m), \mathrm{v}_{0my} = a_m \sin(t_m), \tag{5}$$

where $t_m = 2\pi(m-1)/(M-1)$ and $a_m = b(m-1)/(M-1)$ denote the rotation angle and the distance from the center, respectively, with b as a constant that is set as 0.48 mm in the following.

The response function of an optical system $H(\mathbf{r}, \mathbf{v})$ is a traditional Fourier transform system, which is expressed as:

$$H(\mathbf{r}, \mathbf{v}) = -\frac{i}{\lambda f} T(\mathbf{r}) \exp\left[\frac{i\pi}{\lambda f}\left(\mathbf{v}^2 - 2\mathbf{r}\cdot\mathbf{v}\right)\right], \tag{6}$$

where λ represents the wavelength, f is the focal length of the Fourier transform lens, and $T(\mathbf{r}) = \exp\left(-\mathbf{r}^2/2\sigma_0^2\right)$ is the amplitude function. By substituting Equations (3), (4), and (6) into Equation (2), we can find the CSD function in the source plane:

$$W(\mathbf{r}_1, \mathbf{r}_2) = \exp\left(-\frac{\mathbf{r}_1^2 + \mathbf{r}_2^2}{2\sigma_0^2}\right) \mu(\mathbf{r}_1, \mathbf{r}_2), \tag{7}$$

where σ_0 denotes the transverse beam waist size and is taken as $\sigma_0 = 1.5$ mm in the following simulations. $\mu(\mathbf{r}_1, \mathbf{r}_2)$ denotes the complex degree of coherence (CDOC), which is calculated

from the Fourier transform of the intensity distribution of the incoherent source $\mathrm{I}(\mathbf{v})$, with the CDOC of the SCLs being

$$\begin{aligned}\mu(\mathbf{r}_1,\mathbf{r}_2) &= \tfrac{1}{\lambda^2 f^2}\int \mathrm{I}(\mathbf{v})\exp\left[-\tfrac{i2\pi\mathbf{v}\cdot(\mathbf{r}_2-\mathbf{r}_1)}{\lambda f}\right]d^2\mathbf{v}\\ &= C_1\sum_{m=1}^{M} c_m \exp\left\{-\tfrac{(\mathbf{r}_2-\mathbf{r}_1)^2}{2\delta_m^2}-\tfrac{ika_m}{f}[\cos(t_m)\cdot(x_2-x_1)+\sin(t_m)\cdot(y_2-y_1)]\right\},\end{aligned} \tag{8}$$

where C_1 is a constant factor, $k = 2\pi/\lambda$ is the wavenumber, and $\delta_m = \lambda f/\pi\omega_m$ denotes the transverse coherence width of the mth spot of the SCLs. The second-order statistical characteristics of SCL can be described by the two-point cross-spectral density function in the source plane:

$$\begin{aligned}W(\mathbf{r}_1,\mathbf{r}_2) &= C_1\exp\left(-\tfrac{\mathbf{r}_1^2+\mathbf{r}_2^2}{2\sigma_0^2}\right)\\ &\times\sum_{m=1}^{M} c_m \exp\left\{-\tfrac{(\mathbf{r}_2-\mathbf{r}_1)^2}{2\delta_m^2}-\tfrac{ika_m}{f}[\cos(t_m)\cdot(x_2-x_1)+\sin(t_m)\cdot(y_2-y_1)]\right\},\end{aligned} \tag{9}$$

where based on Equation (9), a uniform spiral coherent lattice (USCL) with $\omega_m \equiv \omega_0$ and a non-uniform spiral coherent lattice (NUSCL) with $\omega_m = \sqrt{m}\omega_0$ can be achieved by manipulating the parameter ω_m, with its transverse coherence width being δ_0 and $\delta_m = \delta_0/\sqrt{m}$.

The paraxial propagation of a coherent lattice is characterized by the generalized Huygens–Fresnel integral, and the CSD function of the beam after propagating through a stigmatic ABCD optical system can be calculated from [41,52]:

$$\begin{aligned}W(\boldsymbol{\rho}_1,\boldsymbol{\rho}_2) &= \tfrac{1}{(\lambda B)^2}\exp\left[-\tfrac{ikD}{2B}\left(\boldsymbol{\rho}_1^2-\boldsymbol{\rho}_2^2\right)\right]\int\int W(\mathbf{r}_1,\mathbf{r}_2)\exp\left[-\tfrac{ikA}{2B}\left(\mathbf{r}_1^2-\mathbf{r}_2^2\right)\right]\\ &\times\exp\left[\tfrac{ik}{B}(\mathbf{r}_1\cdot\boldsymbol{\rho}_1-\mathbf{r}_2\cdot\boldsymbol{\rho}_2)\right]d^2\mathbf{r}_1 d^2\mathbf{r}_2,\end{aligned} \tag{10}$$

where $\boldsymbol{\rho}_1$ and $\boldsymbol{\rho}_2$ are two arbitrary transverse position vectors at the output plane. A, B, C, and D are the transfer matrix elements of the optical system. The intensity and CDOC of the SCLs in the output plane are obtained as [53]:

$$I(\boldsymbol{\rho}) = W(\boldsymbol{\rho},\boldsymbol{\rho}), \tag{11}$$

$$\mu(\boldsymbol{\rho}_1,\boldsymbol{\rho}_2) = \frac{W(\boldsymbol{\rho}_1,\boldsymbol{\rho}_2)}{\sqrt{I(\boldsymbol{\rho}_1)I(\boldsymbol{\rho}_2)}}, \tag{12}$$

Assuming that the SCLs pass through a thin lens, the propagation properties can be studied with the help of the transfer matrix of the optical system between the source plane and the output plane, which is written as:

$$\begin{pmatrix}A & B\\ C & D\end{pmatrix} = \begin{pmatrix}1 & z\\ 0 & 1\end{pmatrix}\begin{pmatrix}1 & 0\\ -1/f_1 & 1\end{pmatrix} = \begin{pmatrix}1-z/f_1 & z\\ -1/f_1 & 1\end{pmatrix}. \tag{13}$$

where z is the distance from the focal lens to the output plane.

In the experiment, we can calculate the square modulus of the CDOC using the following formula. As the light transmitted through the rotating ground glass disk obeys Gaussian statistics, by applying the Gaussian moment theorem, we can express the square modulus of the CDOC of the beam in the output plane using the intensity correlation expression, as follows [53]:

$$|\mu(\mathbf{r}_1,\mathbf{r}_2)|^2 = \frac{N\sum_n^N I_n(\mathbf{r}_1)I_n(\mathbf{r}_2)}{\sum_n^N I_n(\mathbf{r}_1)\sum_n^N I_n(\mathbf{r}_2)} - 1, \tag{14}$$

Here, N is the number of ensemble realizations and $I_n(\mathbf{r})$ is an intensity distribution of the n-th realization.

As discussed in the following section of the paper, we set $c_m = 1$ to simplify our simulations, but this is still a useful parameter for the flexible and programmable construction of the partially coherent optical array.

3. Results and Discussion

In this section, we not only theoretically simulated the evolutionary characteristics of normalized intensity distributions and the square modulus of CDOC distributions of SCLs during propagation using the proposed method in the article, but also verified the feasibility of our method in experiments.

Figure 1 shows the normalized intensity distribution $\mathrm{I}(\mathbf{v})/\mathrm{I}(\mathbf{v})_{\max}$ of the incoherent light, the square modulus, and its phase of the CDOC of USCLs in the source plane with $\delta_0 = 1$ mm, for different spot numbers M. The incoherent spiral intensity from a discrete distribution gradually turns into a continuous structure, with the increase in the total spots of number M (see Figure 1(a1–d1)). Amazingly, the square modulus of the CDOC distribution in the source plane also shows a spiral shape, and the spiral shape of the CDOC distribution in the source plane becomes continuous as the number of spots M increases for USCLs (see Figure 1(a2–d2)), with its phase consisting of singularity arrays (see Figure 1(a3–d3)) and gradually turning into a continuous shape as M increases. The generation of phase singularities in this article is caused by correlated singularities which are caused by the discontinuity of the light field distribution. This can be seen from Equation (8) in the article. Equation (8) for CDOC distribution is a $\sum$ sum form, resulting in discontinuity. This is different from the fact that the phase singularity of a typical vortex beam is caused by the generation of the vortex phase. From the figure, we can see that the phase distribution of CDOC of USCLs gradually becomes clear with M increases and we can manipulate the number of phase singularities and distributions by adjusting the total number of M spots.

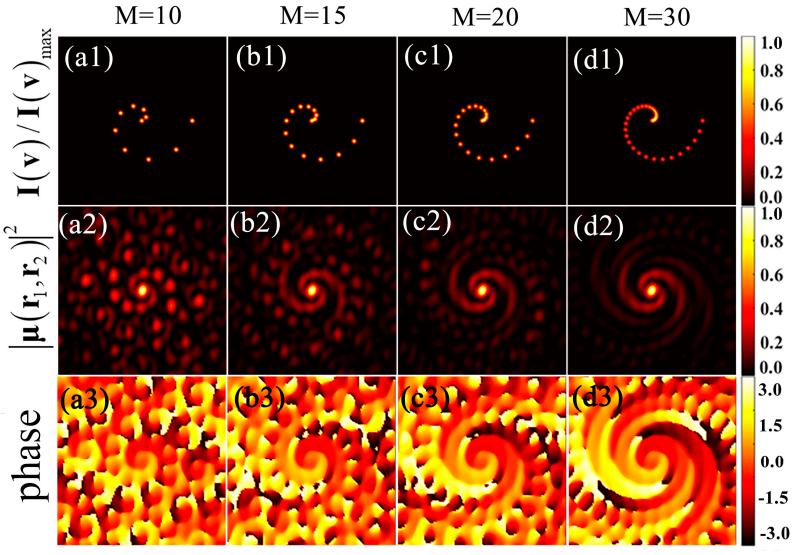

Figure 1. Density plots of (**a1–d1**) the normalized intensity distribution $\mathrm{I}(\mathbf{v})/\mathrm{I}(\mathbf{v})_{\max}$ of the incoherent light for generating USCLs, (**a2–d2**) the square modulus of the CDOC, and (**a3–d3**) its phase distribution of the CDOC of the USCLs with $\delta_0 = 1$ mm, for different spot numbers M.

Figure 2 show the normalized intensity distribution $\mathrm{I}(\mathbf{v})/\mathrm{I}(\mathbf{v})_{\max}$ of the incoherent light, the square modulus, and its phase of the CDOC of NUSCLs in the source plane with $\delta_0 = 1$ mm, for different spot numbers M; a much more continuous shape can be achieved by manipulating the beam waist size ω_m, showing a great difference between the USCLs and NUSCLs. The incoherent spiral intensity from a discrete distribution gradually turns into a

continuous structure by manipulating the beam waist size ω_m and the total spots of number M (see Figure 1(a1–d1) and Figure 2(a1–d1)). The square modulus of the CDOC distribution in the source plane also shows a spiral shape in the source plane which is similar to the USCLs; the spiral shape of the CDOC distribution in the source plane becomes continuous as the number of spots M increases for NUSCLs, compared with the USCLs, and the square modulus of the CDOC distribution of NUSCLs has fewer side lobes (see Figure 1(a2–d2) and Figure 2(a2–d2)), with its phase consisting of singularity arrays, and gradually turns into a continuous shape as M increases. The phase singularities show a clearer distribution than USCLs (see Figure 1(a3–d3) and Figure 2(a3–d3)). The phase distribution of CDOC of NUSCLs gradually becomes clear with M increases, which is similar to USCLs, but phase distributions of the CDOC of NUSCLs are clearer and more compact compared with the USCLs. Additionally, one can not only introduce phase singularities through a vortex phase [54,55] but also through constructing coherent lattices appropriately, and its phase distribution can be manipulated by the beam parameters, e.g., the spots number M and the beam waist size ω_m, flexibly. The spiral coherent lattices are only an example of our flexible construction of the partially coherent optical array. Through our method, various optical coherent arrays can be obtained.

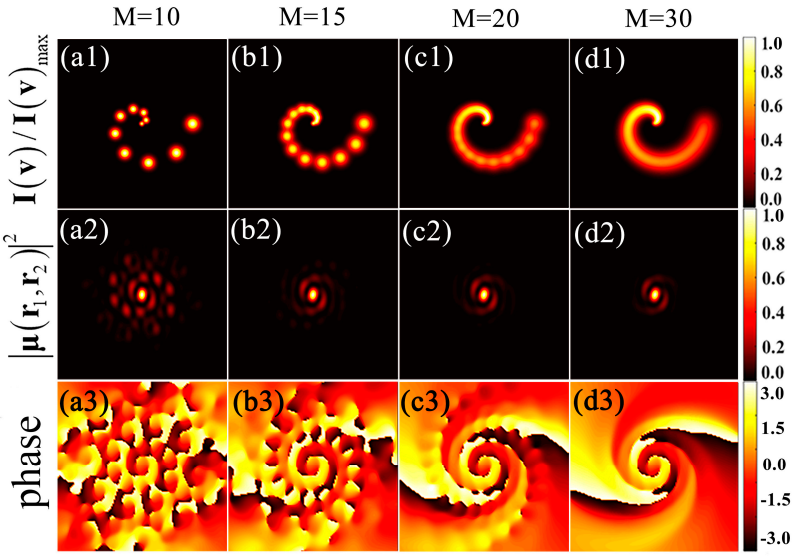

Figure 2. Density plots of (**a1–d1**) the normalized intensity distribution $\mathrm{I}(\mathbf{v})/\mathrm{I}(\mathbf{v})_{\max}$ of the incoherent light for generating NUSCLs, (**a2–d2**) the square modulus of the CDOC, and (**a3–d3**) its phase distribution of the CDOC of the NUSCLs with δ_0 = 1 mm for different spot numbers M.

The density plots of the normalized intensity and its square modulus of the CDOC of the SCLs after propagation through a thin lens with a focal length of f_1 = 400 mm are shown in Figure 3. The figure shows that the SCLs gradually evolve from a Gaussian distribution to an SCL structure during propagation (see Figure 3(a1–d1,a3–d3)). The evolution of the intensity distribution of the SCLs is similar to the exponential phase beams, with the intensity distribution changing from a symmetric distribution to an asymmetric distribution gradually during propagation. The physical mechanism can be explained by the symmetry-breaking structure of the phase distribution, i.e., the original axial symmetry of the beam in the focal plane is disrupted by the introduced nonuniform spiral phase. Not only does the center of gravity of the intensity shift, but the energy flux distribution in the focal plane also changes significantly [56,57]. The SCLs have a similar phase distribution to the exponential phase beams, with the phase of the CSD function consisting of the offset superposition phase terms (see Equation (9)). Therefore, discrete (or uniform) and continuous (or nonuniform) exponential phase-like beams can be achieved by modulating the SCLs. The corresponding square modulus of the CDOC is plotted in Figure 3(a2–d2,a4–d4). We found that the square modulus of the CDOC of USCLs in the source plane has a shape similar to a windmill, and

the square modulus of the CDOC in windmill shape rotates during propagation, which is interesting. Compared with the USCLs, the square modulus of the CDOC of NUSCLs shows fewer sidelobes, although the square modulus of the CDOC will rotate during propagation, too. The distribution of the square modulus of the CDOC of SCLs evolves from a spiral shape to a Gaussian distribution, and rotation occurs during propagation, with the sidelobes gradually degrading. Compared to the USCLs, the square modulus of the CDOC of an NUSCLs has a pure background, which is helpful when used as the freedom to load information. Two types of spiral coherent lattices have been studied, which included USCLs and NUSCLs, and their arrangement is the same, but there is a difference in the size of the light spot. It should be noted that the SCLs are only an example proposed for our method, and various coherent lattice structures can be generated by this flexible and programmable method.

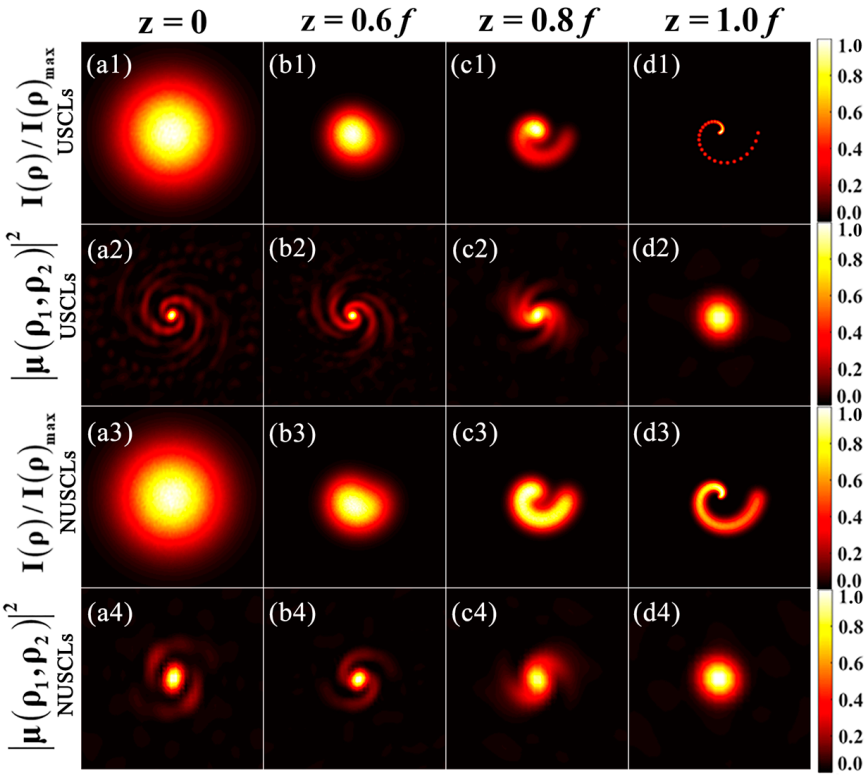

Figure 3. Density plots of (**a1**–**d1**) and (**a3**–**d3**), the normalized intensity distribution $I(\boldsymbol{\rho})/I(\boldsymbol{\rho})_{max}$, and (**a2**–**d2**) and (**a4**–**d4**), the square modulus of the CDOC of the focused USCLs and NUSCLs, at several propagation distances z, with δ_0 = 1 mm and M = 30.

The density plots of the normalized intensity distribution of the SCLs with different transverse coherence widths in the focal plane after passing through a thin lens with a focal length of f_1 = 400 mm are shown in Figure 4. Uniform (see Figure 4(a1–d1)) and nonuniform (see Figure 4(a2–d2)) lattice distributions in the focal plane can be observed gradually with the increase in the transverse coherence width. Additionally, the focal plane intensity distribution of the NUSCLs is more uniform than that of the USCLs with a lower transverse coherence width (see Figure 4(a1,a2)). These phenomena can be explained based on Equation (9). The distribution of the CDOC is determined by the Gaussian term and the Schell-mode term, in contrast to that of the USCLs, and the NUSCLs with the Schell-model terms are modulated by the parameter m, i.e., Schell-model terms decrease with the increase in m, and the phase term is the same as that of the USCLs. The influence of the Gaussian amplitude of the CDOC is small when utilizing the modulation parameter m with a lower transverse coherence width. A clear lattice distribution of the SCLs can be observed (see Figure 4(d1,d2)), with a higher transverse coherence width because the Gaussian terms

play a main role in the CDOC functions. The influence of the modulation parameter m is smaller with a higher transverse coherence width. This proves that we can not only manipulate its spatial coherence structure to achieve beam shaping, but also adjust its transverse coherence width to achieve beam shaping for the partially coherent optical array that we have constructed. And this undoubtedly increases the flexibility of regulation.

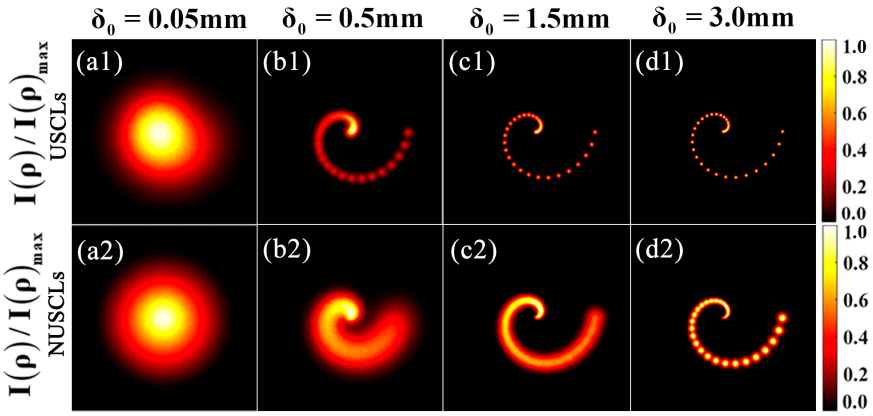

Figure 4. Density plots of the normalized intensity distribution $I(\rho)/I(\rho)_{max}$ of the focused (**a1**–**d1**) USCLs and (**a2**–**d2**) NUSCLs in the focal plane with M = 30 for different transverse coherence widths δ_0.

To prove the feasibility of our approach, we utilized the experimental schematic shown in Figure 5. A linear polarized laser beam with a wavelength of λ= 532 nm from a Nd:YAG laser is expanded by a beam expander (BE), and modulated by a spatial light modulator (SLM) with a computer-generated hologram (CGH). Figure 5 illustrates the CGH used to generate the SCLs after passing through a beam splitter (BS). The generated beam from the SLM is then emitted to dynamic scattering, e.g., a rotating ground glass disk (RGGD), producing an incoherent light field, after being collimated and filtered by the thin lens L_2 (f_2 =150 mm) and Gaussian amplitude filter (GAF). This generates the SCLs source, and the distance from the RGGD to the thin lens L_2 is 15 cm. The transverse coherence width can be adjusted utilizing the distance from the thin lens L_1 to RGGD. A neutral density filter (NDF) is used to adjust the amplitude of the laser beam. The generated SCLs are then split into two parts, with the transmitted part passing through a $4f$ image system, consisting of thin lenses L_3 and L_4 with a focal length of $f_3 = f_4 = f$ = 150 mm, and are then recorded by a charge-coupled device (CCD_1). The reflected part is focused by a thin lens L_5 and then received by a charge-coupled device (CCD_2) which is located at a distance z from the thin lens L_5. The recorded frames from the CCDs are used to measure the intensity and the square modulus of the CDOC in the source plane and propagated plane, respectively. For the measurement of the square modulus of the CDOC of the partially coherent optical array, we can refer to Equation (14).

Figure 6 shows our experimental results of the normalized intensity distribution and the square modulus of the CDOC of the USCLs and NUSCLs at several propagation distances z with M = 30 and δ_0 = 1 mm. By using CCD camera, we obtained its intensity distribution, and by performing calculations on the intensity correlation, we obtained the square modulus of the CDOC of the SCLs. Consistent with our theoretical simulation, the intensity distribution of SCLs gradually evolves from a Gaussian distribution to a coherent lattice during propagation, and the square modulus of the CDOC gradually rotates during propagation and eventually evolves into a Gaussian distribution when reaching the far field. Usually, we approximate the focal plane after it has been focused by a lens as a far-field plane. The results of the measurements are in good agreement with the simulation results shown in Figure 3, whether for intensity distribution or the square modulus of the CDOC distribution. This also confirms the correctness of our method.

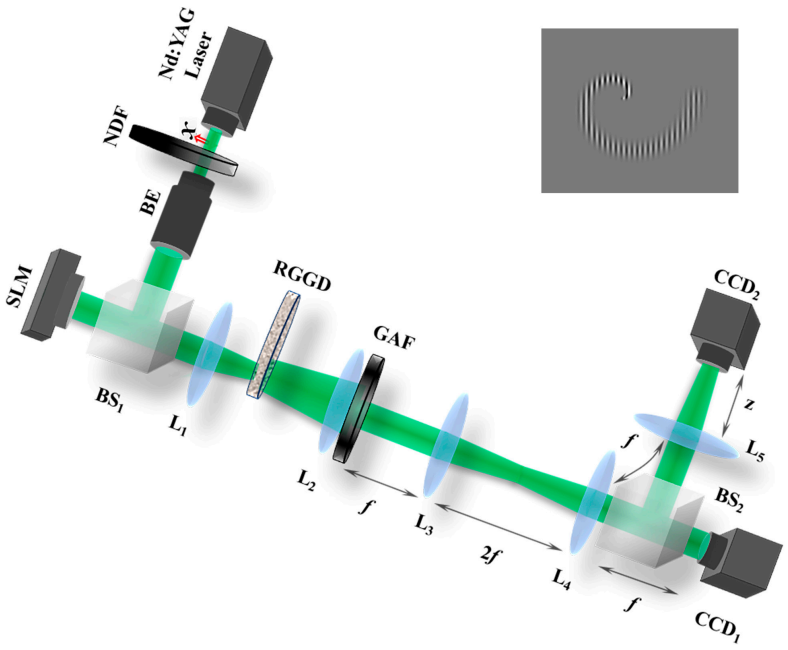

Figure 5. Experimental setup for the generation and measurement of the SCLs. NDF, neutral density filter; BE, beam expander; BS_1 and BS_2, beam splitters; SLM, spatial light modulator; RGGD, rotating ground-glass disk; L_1, L_2, L_3, L_4 and L_5, thin lenses; GAF, Gaussian amplitude filter; CCD_1 and CCD_2, charge-coupled devices.

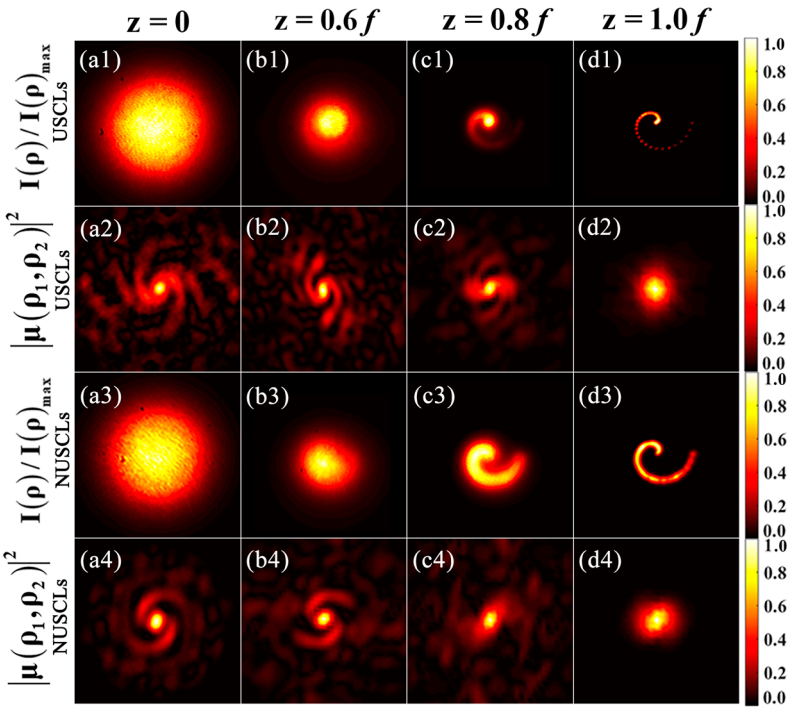

Figure 6. Experimental measurements of (**a1**–**d1**) and (**a3**–**d3**), the normalized intensity distribution $I(\rho)/I(\rho)_{max}$, and (**a2**–**d2**) and (**a4**–**d4**), the square modulus of the CDOC of the focused USCLs and NUSCLs, at several propagation distances z with δ_0 = 1 mm and M = 30.

Figure 7 shows the experimental measurement of the intensity distribution of the USCLs and NUSCLs in the focal plane. Various intensity distributions, e.g., Gaussian, Gaussian-like, discrete or continuous spiral-like, and uniform or nonuniform coherence lattice distributions in the focal plane can be generated by manipulating the transverse

coherence width and the initial coherence structure. The experimental results of Figure 7 correspond well with the theoretical simulation of Figure 4.

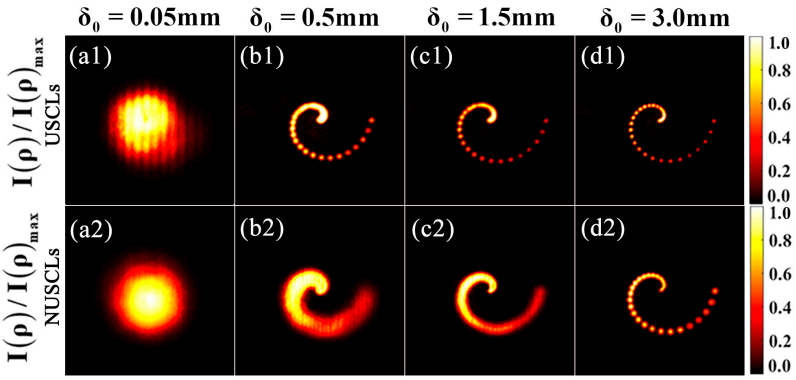

Figure 7. Experimental measurements of (**a1**–**d1**), the normalized intensity distribution of the USCLs, and (**a2**–**d2**), the NUSCLs in the focal plane, for different transverse coherence widths δ_0 with M = 30.

4. Conclusions

In summary, we propose a programmable method for the flexible construction of an optical array, with a variety of manipulated parameters, e.g., the amplitude or the size of individual light spots, the number of light spots, the relative position of the light spots, etc. Two types of spiral coherent lattices, USCLs and NUSCLs, have been studied to verify the feasibility of our method. SCLs and their propagation properties are investigated as an example, both theoretically and experimentally. The intensity of the SCLs evolves from a Gaussian distribution to coherent lattices. Additionally, one can obtain Gaussian, Gaussian-like, and various coherence lattices by manipulating the transverse coherence width and the parameters of the lattice structures. In addition, the distribution of the square modulus of the CDOC of SCLs evolves from a spiral shape to a Gaussian distribution, and rotation occurs during propagation. Surprisingly, the phase of the CDOC of the SCLs exhibits phase singularities in the source plane, which can be used for the construction of optical vortex beams. Our method provides powerful, convenient, and economical tools for applications such as multiparticle capture and manipulation, material processing, and free-space optical communications, and has great significance for extending the theory and application of light beams.

Author Contributions: Conceptualization, K.Z. and X.L. (Xianlong Liu); methodology, Y.W.; software, K.Z.; validation, X.L. (Xianlong Liu), K.Z. and M.L.; investigation, K.Z.; data curation, K.Z.; writing—original draft preparation, K.Z. and X.L. (Xiaofei Li); writing—review and editing, X.L. (Xianlong Liu) and X.L. (Xiaofei Li); supervision, X.L. (Xianlong Liu) and Y.G.; project administration, X.L. (Xianlong Liu) and Y.G.; funding acquisition, X.L. (Xianlong Liu). All authors have read and agreed to the published version of the manuscript.

Funding: This research was funded by the National Natural Science Foundation of China (Grant Nos. 12274268 and 11904211).

Institutional Review Board Statement: Not applicable.

Informed Consent Statement: Not applicable.

Data Availability Statement: Data are contained within the article.

Conflicts of Interest: The authors declare no conflicts of interest.

References

1. Gori, F.; Santarsiero, M. Devising genuine spatial correlation functions. *Opt. Lett.* **2007**, *32*, 3531–3533. [CrossRef]
2. Gori, F.; Ramírez-Sánchez, V.; Santarsiero, M.; Shirai, T. On genuine cross-spectral density matrices. *J. Opt. A Pure Appl. Opt.* **2009**, *11*, 085706. [CrossRef]

3. Li, T.; Zhang, X.; Huang, K.; Lu, X. Experimental generation of partially coherent circular Airy beams. *Opt. Laser Technol.* **2021**, *137*, 106814. [CrossRef]
4. Seshadri, S.R. Average characteristics of a partially coherent Bessel—Gauss optical beam. *J. Opt. Soc. Am. A* **1999**, *16*, 2917–2927. [CrossRef]
5. Chen, Y.; Liu, L.; Wang, F.; Zhao, C.; Cai, Y. Elliptical Laguerre-Gaussian correlated Schell-model beam. *Opt. Express* **2014**, *22*, 13975–13987. [CrossRef]
6. Wang, F.; Liang, C.; Yuan, Y.; Cai, Y. Generalized multi-Gaussian correlated Schell-model beam: From theory to experiment. *Opt. Express* **2014**, *22*, 23456–23464. [CrossRef]
7. Li, X.; Wei, H.; Visser, T.D.; Cai, Y.; Liu, X. Partially coherent perfect vortex beam generated by an axicon phase. *Appl. Phys. Lett.* **2021**, *119*, 171108. [CrossRef]
8. Dong, M.; Zhao, C.; Cai, Y.; Yang, Y. Partially coherent vortex beams: Fundamentals and applications. *Sci. China Phys. Mech. Astron.* **2021**, *64*, 224201. [CrossRef]
9. Liu, Y.; Dong, Z.; Chen, Y.; Cai, Y. Research advances of partially coherent beams with novel coherence structures: Engineering and applications. *Opto-Electron. Eng.* **2022**, *49*, 220178.
10. Yu, J.; Zhu, X.; Lin, S.; Wang, F.; Gbur, G.; Cai, Y. Vector partially coherent beams with prescribed non-uniform correlation structure. *Opt. Lett.* **2020**, *45*, 3824–3827. [CrossRef]
11. Wang, H.; Peng, X.; Zhang, H.; Liu, L.; Chen, Y.; Wang, F.; Cai, Y. Experimental synthesis of partially coherent beam with controllable twist phase and measuring its orbital angular momentum. *Nanophotonics* **2022**, *11*, 689–696. [CrossRef]
12. He, Q.; Turunen, J.; Friberg, A.T. Propagation and imaging experiments with Gaussian Schell-model beams. *Opt. Commun.* **1988**, *67*, 245–250. [CrossRef]
13. Cai, Y.; Chen, Y.; Yu, J.; Liu, X.; Liu, L. Chapter Three—Generation of Partially Coherent Beams. *Prog. Opt.* **2017**, *62*, 157–223.
14. Zhou, Y.; Cui, Z.; Han, Y. Polarization and coherence properties in self-healing propagation of a partially coherent radially polarized twisted beam. *Opt. Express* **2022**, *30*, 23448–23462. [CrossRef]
15. Ding, C.; Koivurova, M.; Turunen, J.; Pan, L. Self-focusing of a partially coherent beam with circular coherence. *J. Opt. Soc. Am. A* **2017**, *34*, 1441–1447. [CrossRef]
16. Chen, Y.; Gu, J.; Wang, F.; Cai, Y. Self-splitting properties of a Hermite-Gaussian correlated Schell-model beam. *Phys. Rev. A* **2015**, *91*, 013823. [CrossRef]
17. Wang, Y.; Mei, Z.; Zhang, M.; Mao, Y. Propagation characteristics of a partially coherent self-shifting beam in random media. *Appl. Opt.* **2020**, *59*, 1834–1840. [CrossRef] [PubMed]
18. Wang, F.; Liu, X.; Cai, Y. Propagation of Partially Coherent Beam in Turbulent Atmosphere: A Review (Invited Review). *Prog. Electromagn. Res.* **2015**, *150*, 123–143. [CrossRef]
19. Huang, X.; Deng, Z.; Shi, X.; Bai, Y.; Fu, X. Average intensity and beam quality of optical coherence lattices in oceanic turbulence with anisotropy. *Opt. Express* **2018**, *26*, 4786–4797. [CrossRef]
20. Zhang, X.; Chen, Y.; Wang, F.; Cai, Y. Scattering of Partially Coherent Vector Beams by a Deterministic Medium Having Parity-Time Symmetry. *Photonics* **2022**, *9*, 140. [CrossRef]
21. Liu, Y.; Zhang, X.; Dong, Z.; Peng, D.; Chen, Y.; Wang, F.; Cai, Y. Robust Far-Field Optical Image Transmission with Structured Random Light Beams. *Phys. Rev. Appl.* **2022**, *17*, 024043. [CrossRef]
22. Ricklin, J.C.; Davidson, F.M. Atmospheric optical communication with a Gaussian Schell beam. *J. Opt. Soc. Am. A* **2003**, *20*, 856–866. [CrossRef]
23. Kermisch, D. Partially coherent image processing by laser scanning. *J. Opt. Soc. Am.* **1975**, *65*, 887–891. [CrossRef]
24. Liu, Y.; Chen, Y.; Wang, F.; Cai, Y.; Liang, C.; Korotkova, O. Robust far-field imaging by spatial coherence engineering. *Opto-Electron. Adv.* **2021**, *4*, 210027. [CrossRef]
25. Wang, M.; Yuan, X.; Ma, D. Potentials of radial partially coherent beams in free-space optical communication: A numerical investigation. *Appl. Opt.* **2017**, *56*, 2851–2857. [CrossRef]
26. Gbur, G.; Visser, T.D. Chapter 5—The Structure of Partially Coherent Fields. *Prog. Opt.* **2010**, *55*, 285–341.
27. Wu, Y.; Mei, H.; Dai, C.; Zhao, F.; Wei, H. Design and analysis of performance of FSO communication system based on partially coherent beams. *Opt. Commun.* **2020**, *472*, 126041. [CrossRef]
28. Forbes, A.; Dudley, A.; McLaren, M. Creation and detection of optical modes with spatial light modulators. *Adv. Opt. Photon.* **2016**, *8*, 200–227. [CrossRef]
29. Guo, L.; Feng, Z.; Fu, Y.; Min, C. Generation of vector beams array with a single spatial light modulator. *Opt. Commun.* **2021**, *490*, 126915. [CrossRef]
30. Streibl, N. Beam Shaping with Optical Array Generators. *J. Mod. Opt.* **1989**, *36*, 1559–1573. [CrossRef]
31. Chen, B.; Legant, W.R.; Wang, K.; Shao, L.; Milkie, D.E.; Davidson, M.W.; Janetopoulos, C.; Wu, X.S.; Hammer, J.A.; Liu, Z.; et al. Lattice light-sheet microscopy: Imaging molecules to embryos at high spatiotemporal resolution. *Science* **2014**, *346*, 1257998. [CrossRef]
32. Schäfer, F.; Fukuhara, T.; Sugawa, S.; Takasu, Y.; Takahashi, Y. Tools for quantum simulation with ultracold atoms in optical lattices. *Nat. Rev. Phys.* **2020**, *2*, 411–425. [CrossRef]
33. Ma, L.; Ponomarenko, S.A. Optical coherence gratings and lattices. *Opt. Lett.* **2014**, *39*, 6656–6659. [CrossRef]

34. Liang, C.; Mi, C.; Wang, F.; Zhao, C.; Cai, Y.; Ponomarenko, S.A. Vector optical coherence lattices generating controllable far-field beam profiles. *Opt. Express* **2017**, *25*, 9872–9885. [CrossRef] [PubMed]
35. Liu, X.; Liu, L.; Peng, X.; Liu, L.; Wang, F.; Gao, Y.; Cai, Y. Partially coherent vortex beam with periodical coherence properties. *J. Quant. Spectrosc. Radiat.* **2019**, *222*, 138–144. [CrossRef]
36. Chen, Y.; Ponomarenko, S.A.; Cai, Y. Experimental generation of optical coherence lattices. *Appl. Phys. Lett.* **2016**, *109*, 061107. [CrossRef]
37. Ma, L.; Ponomarenko, S.A. Free-space propagation of optical coherence lattices and periodicity reciprocity. *Opt. Express* **2015**, *23*, 1848–1856. [CrossRef]
38. Liu, X.; Yu, J.; Cai, Y.; Ponomarenko, S.A. Propagation of optical coherence lattices in the turbulent atmosphere. *Opt. Lett.* **2016**, *41*, 4182–4185. [CrossRef]
39. Jin, Y.; Wang, H.; Liu, L.; Chen, Y.; Wang, F.; Cai, Y. Orientation-selective sub-Rayleigh imaging with spatial coherence lattices. *Opt. Express* **2022**, *30*, 9548–9561. [CrossRef]
40. Liang, C.; Liu, X.; Xu, Z.; Wang, F.; Wen, W.; Ponomarenko, S.A.; Cai, Y.; Ma, P. Perfect optical coherence lattices. *Appl. Phys. Lett.* **2021**, *119*, 131109. [CrossRef]
41. Liu, Y.; Dong, Z.; Wang, F.; Chen, Y.; Cai, Y. Generation of a higher-order Poincare sphere beam array with spatial coherence engineering. *Opt. Lett.* **2022**, *47*, 5220–5223. [CrossRef]
42. Liu, X.; Zeng, J.; Cai, Y. Review on vortex beams with low spatial coherence. *Adv. Phys. X* **2019**, *4*, 1626766. [CrossRef]
43. Liu, L.; Gao, Y.; Liu, X. High-dimensional vortex beam encoding/decoding for high-speed free-space optical communication. *Opt. Commun.* **2019**, *452*, 40–47. [CrossRef]
44. Zhang, H.; Li, J.; Guo, M.; Duan, M.; Feng, Z.; Yang, W. Optical trapping two types of particles using a focused vortex beam. *Optik* **2018**, *166*, 138–146. [CrossRef]
45. Béché, A.; Juchtmans, R.; Verbeeck, J. Efficient creation of electron vortex beams for high resolution STEM imaging. *Ultramicroscopy* **2017**, *178*, 12–19. [CrossRef] [PubMed]
46. Anzolin, G.; Tamburini, F.; Bianchini, A.; Umbriaco, G.; Barbieri, C. Optical vortices with starlight. *Astron. Astrophys.* **2008**, *488*, 1159–1165. [CrossRef]
47. Sueda, K.; Miyaji, G.; Miyanaga, N.; Nakatsuka, M. Laguerre-Gaussian beam generated with a multilevel spiral phase plate for high intensity laser pulses. *Opt. Express* **2004**, *12*, 3548–3553. [CrossRef]
48. Khonina, S.N.; Ustinov, A.V.; Logachev, V.I.; Porfirev, A.P. Properties of vortex light fields generated by generalized spiral phase plates. *Phys. Rev. A* **2020**, *101*, 043829. [CrossRef]
49. Zheng, C.; Liu, J.; Li, H.; Wang, M.; Zang, H.; Zhang, Y.; Yao, J. Terahertz metasurface polarization detection employing vortex pattern recognition. *Photon. Res.* **2023**, *11*, 2256–2263. [CrossRef]
50. Huo, P.; Zhang, C.; Zhu, W.; Liu, M.; Zhang, S.; Zhang, S.; Chen, L.; Lezec, H.J.; Agrawal, A.; Lu, Y.; et al. Photonic Spin-Multiplexing Metasurface for Switchable Spiral Phase Contrast Imaging. *Nano Lett.* **2020**, *20*, 2791–2798. [CrossRef]
51. Huang, Q.; Lu, X.; Zhang, H.; Wang, Z.; Yang, Y.; Zhan, Q.; Cai, Y.; Zhao, C. Economical generation of high-quality optical vortices with gradual-width Fermat spiral slit mask. *Sci. China Phys. Mech. Astron.* **2023**, *66*, 244211. [CrossRef]
52. Lin, Q.; Cai, Y. Tensor ABCD law for partially coherent twisted anisotropic Gaussian-Schell model beams. *Opt. Lett.* **2002**, *27*, 216–218. [CrossRef]
53. Liu, X.; Wu, T.; Liu, L.; Zhao, C.; Cai, Y. Experimental determination of the azimuthal and radial mode orders of a partially coherent LGpl beam (Invited Paper). *Chin. Opt. Lett.* **2017**, *15*, 030002.
54. Liu, M.; Chen, J.; Zhang, Y.; Shi, Y.; Zhao, C.; Jin, S. Generation of coherence vortex by modulating the correlation structure of random lights. *Photon. Res.* **2019**, *7*, 1485–1492. [CrossRef]
55. Wang, L.; Wang, L.; Zhu, S. Formation of optical vortices using coherent laser beam arrays. *Opt. Commun.* **2009**, *282*, 1088–1094. [CrossRef]
56. Guo, L.; Xia, T.; Xu, Y.; Xiong, Y.; Leng, X.; Tao, S.; Tian, Y.; Cheng, S. Spoon-like Beams Generated with Exponential Phases. *Coatings* **2022**, *12*, 322. [CrossRef]
57. Xie, G.F.; Li, P.; Liu, S.; Zhao, J.L. Focusing Properties of Symmetric Broken Azimuthally Polarized Beams Modulated by Non-uniform Spiral Phases. *Guangzi Xuebao Acta Photonica Sin.* **2015**, *44*, 17–22.